Warm and cold gas in low-mass protostars : Herschel Space Observatory and ground-based surveys

Yildiz, U

1 *Introduction*

1.1 Low-mass star formation

The query of where we come from or how our Solar System formed are ancient questions. During human history, many different types of people including philosophers, religious leaders, and scientists have tried to come up with different suggestions to address these questions. Today, even with our advanced engineering tools and our improved scientific methods, we are still trying to find at least some clues. Especially after the invention of radio astronomy in the 1930s by Karl Jansky and the detection of the first molecule –the methylidyne radical (CH)– in the interstellar medium in 1937 by optical absorption lines (Swings & Rosenfeld 1937, McKellar 1940), a lot of progress has been made during the course of time. Many new molecules have been discovered in a variety of astronomical sources, which span a large range of conditions.

The Sun is a G2 V-type main-sequence star comprising about 99.86% of the total mass of the Solar System. It largely consists of simple elements, like hydrogen and helium. Molecules, including some complex ones, are found throughout our Solar System. Most importantly, planets like our Earth and their atmospheres contain species like water that are key to the origin of life. To better understand their formation, low-mass stars similar to our Sun need to be studied at different evolutionary stages. This thesis addresses the *formation of the earliest stages of low-mass protostars*.

1.1.1 Molecular clouds

Two forces in the Universe play an important role in the birth and death of the celestial sources. These are: first, *gravity*, which tends to compress material and second, *pressure*, which oppositely pushes the interstellar material apart. At the very outset of star formation, in order for a cloud to collapse, the force of *gravity* must overcome the *thermal pressure* so that the clouds must be cold. The only regions in the *interstellar medium* that are dense enough for the force of gravity to overcome the relatively weak thermal pressure from low gas temperature and thus to allow star formation are the *dark molecular clouds*.

The simplest of those clouds are the *Bok globules*. Their temperatures are around 10 K, the densities range from 10^4 to 10^5 cm^{-3}, and their masses range from 10 to 100 $M_\odot$. While Bok globules have typical sizes of a few parsec, dark clouds or cloud complexes can be significantly larger with sizes of tens of parsecs. These places are the ideal sites for low-mass star formation. Due to the high extinction ($A_V > 100$ mag), the earliest protostellar phase can only be observed at longer wavelengths, e.g., far-infrared, submillimeter, and millimeter. Fig. 1.1 shows the *Herschel* Space Observatory image of the Eagle Nebula (also known as the Pillars of Creation) taken with the PACS/SPIRE instruments. The three color composite image shows the areas of active star birth, where the tips of the pillars also contain protostars. In our Milky Way galaxy, there are many similar molecular clouds that harbor star-forming regions, which form new stars with planets surrounding them.

Observations show that stars form in these collapsing dense and dark molecular clouds either in *isolated* or in *clustered* environments (reviews by Shu et al. 1987, Bergin & Tafalla 2007, Kennicutt & Evans 2012). The outcome of the star formation process may depend on this initial environment. For example, clusters of massive stars together with thousands of low mass stars are formed in giant molecular clouds (GMCs) like those in Orion. However, isolated low-mass stars form in smaller condensations, e.g., B68 in the Pipe Nebula.

Figure 1.1 – *Herschel*-PACS/SPIRE image of the Eagle Nebula. This is a three colour composite with colours assigned as (blue=70μm, green=160μm, red=250μm). The 70 μm and 160 μm data are from PACS and the 250 μm from SPIRE. Credits: ESA/PACS & SPIRE Consortium, T. Hill, F. Motte, CEA/IRFU - CNRS/INSU - Uni. Paris Diderot, HOBYS Key Program Consortium.

1.1.2 Stages of young stellar objects

Low-mass YSOs have been classified by various methods, e.g., based on the infrared slope, $\alpha_{\rm IR} = d\log(\lambda F_\lambda)/d\log\lambda$, of the spectral energy distribution at wavelengths from 2 μm to 20 μm (Lada & Wilking 1984),

$$\alpha_{\rm IR}: \overset{\text{Stage I}}{\longrightarrow} 0.3 \overset{\text{Flat}}{\longrightarrow} -0.3 \overset{\text{Stage II}}{\longrightarrow} -1.6 \overset{\text{Stage III}}{\longrightarrow} \tag{1.1}$$

or based on their bolometric temperature $T_{\rm bol}$, (Myers & Ladd 1993, Chen et al. 1995),

$$T_{\rm bol}: \overset{\text{Class 0}}{\longrightarrow} 70\ {\rm K} \overset{\text{Class I}}{\longrightarrow} 650\ {\rm K} \overset{\text{Class II}}{\longrightarrow} 2800\ {\rm K} \overset{\text{Class III}}{\longrightarrow} \tag{1.2}$$

This sequence reflects that with the evolution of the protostellar phase from molecular clouds to protoplanetary disks, the peak emission shifts from longer to shorter wavelengths.

According to Lada (1987) and André et al. (2000), YSOs are characterized by four different evolutionary classes (Class 0–III) during their formation (Fig. 1.2; Evans et al. 2009, Dunham et al. 2013).

Class 0 — is the earliest and deeply-embedded stage of YSOs, where the *protostar* is surrounded by a collapsing *envelope* and a *circumstellar disk*, from which material is accreted onto the protostar. The mass of the envelope is much larger than that of the central protostar ($M_{\rm env} >> M_*$) and the lifetime of this stage is typically 10^4 - 10^5 years. Very strong *jets* and *winds* erupt from both poles of the protostars and inner disks, which push and entrain the material in the envelope outward

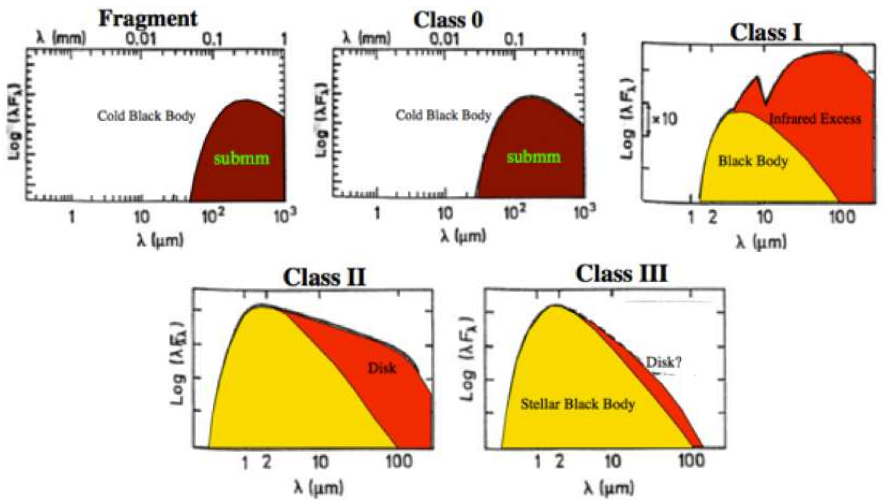

Figure 1.2 – Low mass star formation sequence according to their evolving SEDs. Adapted from André et al. (2000).

Figure 1.3 – Artist impression of the birth of a star. With submillimeter instruments, it is possible to penetrate the surrounding dust of a forming star. While matter accretes on the protostar, bipolar jets and molecular outflows erupt on both sides. Image credit: NASA/JPL-Caltech.

in the form of a collimated *outflow*. These outflows are important for removing angular momentum and mass and helping the accretion process to be more efficient (Fig. 1.3; e.g., Tafalla et al. 2000, Arce et al. 2007). The interaction of the outflows with the surrounding envelope also heats up the material and leads to the formation of many molecules. The spectral energy distribution (SED) of this phase peaks at far-infrared and submillimeter wavelengths.

Class I — is the next stage in the evolution, where the envelope is being dispersed by the outflows while the circumstellar disk grows. This phase lasts a few $\times 10^5$ years and the mass of the envelope is now less than the central protostar ($M_* > M_{\rm env}$). The bipolar outflows are still seen in this stage, however their strength is much lower than in the Class 0 phase. Due to the lower extinction, the SED now consists of two components; blackbody emission from the protostar and infrared excess from the surrounding disk.

Class II — is the phase where the envelope is almost completely dissipated into the protostellar disk ($M_{\rm disk} > M_{\rm env}$). The lifetime of this phase is a few $\times 10^6$ years and the black body radiation is shifted to near-infrared wavelengths, while the disk emission is still seen in the mid-to far-infrared wavelengths. The sources which are observed in this phase are also called *Classical T Tauri stars* (CTTSs), with possible *planet* formation.

Class III — is the phase where the accretion stops and the jets and outflows are entirely gone (Walter 1987). The sources are called *Weak-line T-Tauri stars* (WTTS) with a debris disk or planetary system that may have formed.

Toward the end of the Class III stage, the turning point of becoming a *star* is reached by burning hydrogen in its core through fusion reactions, which then leads to the *hydrostatic equilibrium* of stars. The new-born star appears in the Hertzsprung-Russell Diagram in its so-called *zero-age main-sequence* (ZAMS) period (Hayashi et al. 1962). After this period, the star joins the main sequence stellar evolution phase, which is very stable due to constant processing of Hydrogen into other elements.

Star-formation is a complex process with the components in each of those stages interacting. A good understanding of them is needed both individually and globally. In this thesis, I focus on the early Class 0 and Class I phases by using observations from ground- and space-based submillimeter telescopes, especially the new *Herschel* Space Observatory. Understanding the structure of molecular outflows, which are an integral part of these phases, has made significant progress over the last few decades since the first discovery in a low-mass protostar "L1551-IRS5" by Snell et al. (1980). Although the formation of jets, winds and outflows is not fully understood, it is thought that they result from the interaction of the magnetic field of the central object with the surrounding circumstellar disk. The amount of gas in the outflows in different temperatures can be traced using CO rotational transition observations (see Sect. 1.2). In this thesis, we quantify the cold (T<100 K) and warm (T>100 K) gas via rotational transitions of CO. The accretion also leads to heating of the surrounding envelope with increasing luminosity, leading to evaporation of the molecules that were frozen out during the earliest cold phases (e.g., van Dishoeck & Blake 1998, Ceccarelli et al. 2007, Caselli & Ceccarelli 2012). These detailed studies of the physical and chemical structure of low–mass protostars are important for a complete understanding of the evolution of young stellar objects (YSOs).

1.2 Molecules

The interstellar medium (ISM) consists of ~99% of gas and 1% dust by mass. Approximately 90% of this gas is in the form of H or H_2, 8% in He and ~1-2% is heavier elements by number. More than 170 different molecular species have been detected in various interstellar and

circumstellar media from nearby objects to distant galaxies. About 50 of those molecules contain 6 or more atoms and are called complex molecules (Herbst & van Dishoeck 2009). Deep inside molecular clouds, most of the carbon is in the form of CO and the hydrogen is in the form of H_2.

The other main constituent of molecular clouds is dust grains, and they typically make up 1% of the cloud by mass. Dust grains are key players when it comes to the chemistry in the sense that their surfaces can act as "*catalysts*" of chemical reactions (Herbst & van Dishoeck 2009). However, in order for the surfaces to aid chemical complexity, molecules need to meet and attach themselves to the surface of a grain, a process which is known as *freeze out*.

In dense clouds, the probability of a molecule to meet a grain surface and stick to it is so high that essentially all molecules except H_2 are frozen out. Typically this requires densities greater than $\sim 10^5$ cm^{-3}; if the density is lower, the time it takes for a molecule to randomly meet a dust grain is longer than the lifetime of molecular clouds and so no or little freeze out takes place (Jørgensen et al. 2005c). When the molecules are stuck to the surface, they can meet and react with other molecules. In particular, this is how water is expected to form, from successive reactions of O, O_2, O_3 with H and H_2 (Tielens & Hagen 1982, Ioppolo et al. 2008, Cuppen et al. 2010).

When dust grains heat up, molecules eventually evaporate depending on the binding energy of the molecule to the surface. H_2 has a very low binding energy and evaporates already at ~4 K, CO and O_2 are slightly more tightly bound and laboratory experiments show that they evaporate at ~20 K (Acharyya et al. 2007). H_2O and CH_3OH have higher binding energies and only thermally evaporate once the grains reach temperaures of 100 K or more. These values are all based on high-quality laboratory experiments carried out under controlled conditions.

The density and temperature constraints imply that the abundances of different molecules vary through the envelopes surrounding the forming protostars (Jørgensen et al. 2002). In this thesis, Chapters 2, 3, 4, and 6 discuss the variation of CO abundances in the protostellar envelopes and demonstrate the necessity of a freeze-out zone below the evaporation temperature of CO.

1.2.1 Molecular transitions

By observing molecules, we obtain information on the physical and chemical conditions of their past, today, and future. These molecules are observed through their discrete energy levels, where the transition between two levels emit or absorb radiation which corresponds to a frequency/wavelength that telescopes can detect. This radiation is like a specific blueprint of each species.

Three types of transitions can be observed: *Electronic Transitions* are the transitions among the electronic quantum states in the atoms or molecules, leading to emission of radiation in the visible and UV part of the spectrum. *Vibrational Transitions* are due to the vibrational states within every electronic state and occur due to the oscillatory motion of the nuclei. Regions with temperatures around ~1000 K emit at infrared wavelengths. *Rotational Transitions* are due to the end-over-end tumbling of the molecule and the torque exerted on the molecular dipole. Regions with temperatures <300 K emit mostly at millimeter and submillimeter wavelengths.

In this thesis, rotational transitions of the CO and O_2 molecules are used to characterize the physics and chemistry of the protostellar environments. Rotational transitions are possible when the atoms in a molecule have different electronegativity, so that it has a permanent dipole moment. CO is an asymmetric molecule with a small permanent dipole moment (0.112 Debye), which radiates in rotational transitions effectively. Homonuclear symmetric molecules, such as H_2, do not have a permanent electric dipole moment and only forbidden quadrupole transitions are possible. The pure rotational and rovibrational transitions of H_2 can be observed in regions with high kinetic temperatures of a few hundred to a few thousand Kelvins, e.g., shocked gas. O_2 is also a homonu-

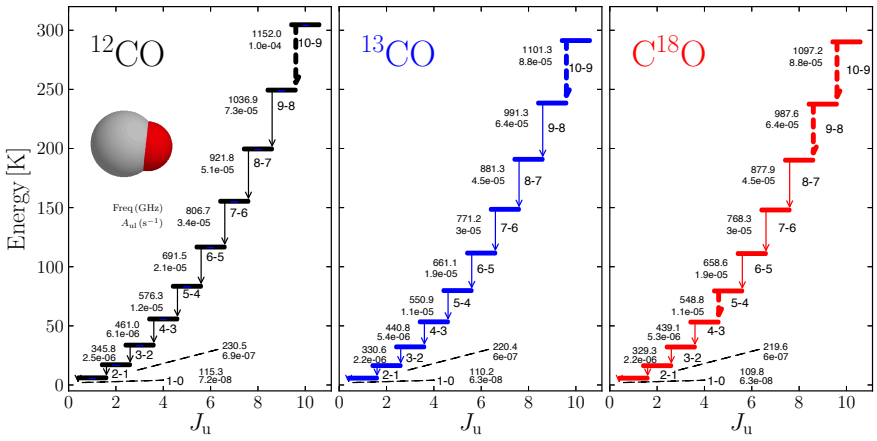

Figure 1.4 – *Right:* ^{12}CO (*left, black*), ^{13}CO (*middle, blue*) and C^{18}O (*right, red*) energy diagrams. Dashed transitions are targeted with *Herschel*-HIFI. The frequencies (in GHz) and Einstein *A* coefficients (in s^{-1}) are also given next to the transitions. Dashed transitions refer to those observed with *Herschel*-HIFI. In this thesis, we use the term "low-*J*" lines to be $J_{up}\leq3$ and "high-*J*" lines with $J_{up}\geq6$.

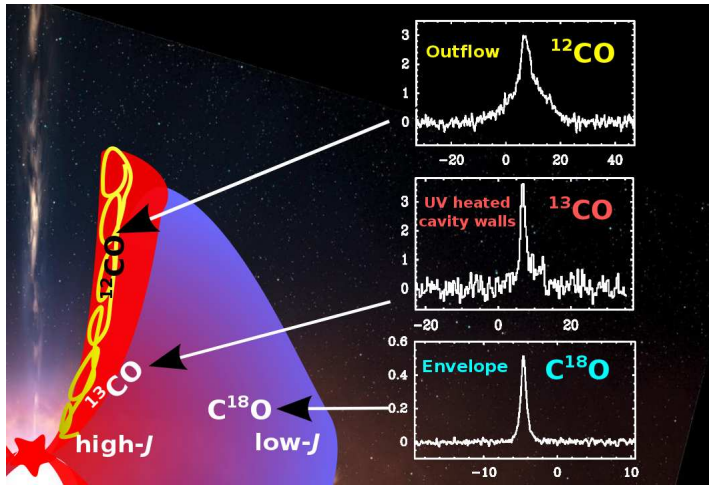

Figure 1.5 – Sketch showing the importance of high angular and spectral resolution to quantify the location and origin of warm and cold gas traced by CO. Background image is adapted from a NASA/JPL-Caltech image.

clear molecule like H_2, but it possesses a magnetic dipole moment, which allows it to radiate weakly at submillimeter wavelengths.

1.2.2 Carbon monoxide - CO

Spectral lines in the millimeter and submillimeter range are tracers of the dense molecular gas, which reveal the kinematic characteristics of collapse in the envelope and the high velocity gas in protostellar outflows. The CO molecule is the second most abundant molecule under most conditions in the interstellar medium after H_2, with a very simple level structure and the different isotopologues (^{13}CO, $C^{18}O$, $C^{17}O$) are detectable at sub-/mm wavelengths. Because of its small dipole moment, CO has the characteristics of being rotationally excited very easily at low densities, and therefore the excitation measurements provide an excellent estimate of the gas kinetic temperature and, by assuming a CO/H_2 abundance, of the molecular gas mass as well. In Fig. 1.4, the energy level diagrams for ^{12}CO, ^{13}CO, and $C^{18}O$ are shown. The rotational levels are more closely spaced than for H_2 because the moment of inertia is greater.

Since its discovery in the Orion molecular cloud (Wilson et al. 1970), CO has served as the primary tracer of molecular gas, both in our own and in external galaxies (e.g., Maloney & Black 1988, Lada 1987, Neininger et al. 1998, Kennicutt & Evans 2012). The most abundant isotope, $^{12}C^{16}O$, is naturally the easiest to detect, but ^{13}CO, $C^{18}O$, and occasionally $C^{17}O$ and $^{13}C^{18}O$, have also proved useful in tracing different environments. Important usage of CO is to characterize the swept-up gas in protostellar outflows where the temperature is relatively low (a few hundred Kelvins). Therefore CO maps have been widely used to identify the physical properties of these outflows. $C^{18}O$ lines are mainly used to probe the quiescent envelope gas, whereas ^{13}CO is found to be good tracer for UV heated gas (Fig. 1.5; Spaans et al. 1995, van Kempen et al. 2009a, Yıldız et al. 2012). In this thesis, Chapters 2–5 discuss the analysis of CO and isotopologue lines observed toward low-mass protostars.

1.2.3 Molecular oxygen - O_2

Oxygen is the third most abundant element in the Universe after hydrogen and helium, but it is still unclear what the main gas-phase reservoir is in dense molecular clouds. It is important to search for O_2 in order to understand the origin of this and other vital molecules for life that are chemically related, such as H_2O. The O_2 in our atmosphere causes strong absorption, therefore interstellar O_2 needs to be observed by space instruments (Goldsmith et al. 2011). In Fig. 1.6, the rotational energy level diagram of O_2 with the corresponding frequencies and Einstein *A* coefficients to each level are presented (adopted from Goldsmith et al. 2011). Until recently, efforts to detect interstellar molecular oxygen had failed due to its very low abundance. Two earlier space missions (*SWAS* and *Odin*) had dedicated instruments to detect O_2, but provided mostly upper limits. *SWAS* did not obtain a definitive detection of O_2 at 487 GHz toward nearby clouds (Goldsmith et al. 2000), whereas *Odin* observations of O_2 at 119 GHz gave upper limits of $\leq 10^{-7}$ (Pagani et al. 2003), except for a tentative detection toward the ρ Ophiuchi A cloud ($X(O_2) \sim 5 \times 10^{-8}$; Larsson et al. 2007).

In the *Herschel* Oxygen Project (HOP) key program, among the seven transitions shown in the Fig. 1.6, three relatively strong transitions at 487, 774, and 1121 GHz were targeted with *Herschel*-HIFI on various star-forming regions and dark clouds, and detected conclusively toward the Orion molecular cloud (Goldsmith et al. 2011) and ρ Ophiuchi A (Liseau et al. 2012). In this thesis, a deep O_2 observation at 487 GHz toward the deeply embedded protostar NGC 1333 IRAS 4A, also studied in CO, is discussed in Chapter 6.

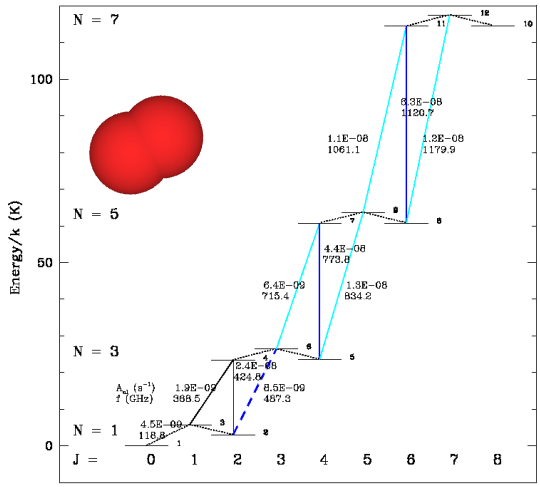

Figure 1.6 – Lower rotational energy level diagram of the O_2 molecule with the corresponding frequencies and Einstein *A* coefficients to each level (Goldsmith et al. 2011). The 487 GHz transition observed with *Herschel* HIFI toward IRAS 4A is shown with dashed blue line. The 774 GHz and 1121 GHz transitions are observed and detected in Orion.

1.3 Observations

In this thesis, observations from different ground- and space-based telescopes were used to obtain the relevant data to study the protostellar environment. The space-based observations are centered on the the *Herschel* Space Observatory, whereas for the ground-based observations, Atacama Pathfinder EXperiment (APEX), James Clerk Maxwell Telescope (JCMT), IRAM 30m telescope, and Onsala 20m Radiotelescope are used. Information about the sample and the observing program (WISH) is given in Sect. 1.4.

1.3.1 *Herschel* Space Observatory

The *Herschel* Space Observatory[1] is a cornerstone mission of European Space Agency (ESA) that aims to study the Universe at far-infrared and submillimeter wavelengths (Pilbratt et al. 2010). Its main objectives are: to study the formation of galaxies in the early universe and their subsequent evolution; study the formation of stars and their interaction with the interstellar medium; observe the chemical composition of the atmospheres and surfaces of comets, planets and satellites; and investigate the molecular chemistry of the universe. The telescope has a Cassegrain design 3.5 meter diameter primary mirror, which is the largest single mirror ever built and launched into space for astronomy to date. The mirror is made of silicon carbide (SiC), which is a ceramic material with a good level of thermal conductivity and a small thermal expansion coefficient (Lemke 2008).

[1] This section is based on the general information over *Herschel* Space Observatory and its instruments, as presented on ESA, NASA and SRON's public web pages.

Herschel was launched together with the *Planck* Observatory from French Guyana by an Ariane–5 rocket on May 14, 2009. Both are currently located in Lissajous orbits about the second Lagrange point of the Sun-Earth system (L2), which is around 1.5 million kilometers away from the Earth. The L2 point is one of the ideal locations, where the observatory uses the Earth's gravity to put the telescope in a stable orbit, and the Earth and the Moon are distant enough to add negligible heating. Having these sources in approximately the same direction as the Sun allows enhanced observation efficiency and flexibility. Its large single-sided radiation shield blocks the thermal radiation from the Sun and the Earth, and by using the fact that space is intrinsically cold allows passive cooling of the telescope mirror to approximately 80 K. The instruments operate at much lower temperatures, which is achieved by cooling via Helium-3 (^{3}He) to reduce the temperature to close to absolute zero temperatures, e.g., 300 mK to use for the PACS and SPIRE bolometers. The HIFI mixers on the other hand operate between 2–4 K.

The liquid helium tank holds 2400 litres, which weighs 335 kg and the whole probe weighs 3.3 tons. The vaporisation rate is 2 mg/sec, meaning that it is aimed to supply a four-year mission with about 7000 hours of science time per year (see review from Lemke 2008). Three science instruments are located in the cryo-vacuum of the helium container, which have different wavelength coverages (Fig. 1.7):

- HIFI (Heterodyne Instrument for the Far Infrared) is a very high resolution heterodyne spectrometer sensitive to 480–1250 and 1410–1910 GHz (157–625 microns) built by a consortium of institutes under leadership of SRON Netherlands Institute for Space Research (Groningen, The Netherlands; de Graauw et al. 2010). The details of this instrument follow in Section 1.3.2.
- PACS (Photodetector Array Camera and Spectrometer) is an imaging photometer and medium resolution grating spectrometer sensitive to the wavelength range from 60 to 210 μm, built under leadership of the Max Planck Institute for Extraterrestrial Physics (Garching, Germany; Poglitsch et al. 2010). PACS consists of 5×5 spatial-pixels (spaxels) with a field-of-view covering 47″ at the resolution of 9.4″.
- SPIRE (Spectral and Photometric Imaging Receiver) is an imaging photometer and an imaging Fourier transform spectrometer sensitive to the wavelength range from 200–670 μm built under leadership of the University of Wales (Cardiff, UK; Griffin et al. 2010).

These instruments complement each other in terms of their capabilities. In this thesis, primarily HIFI observations are used, therefore the following section continues with detailed information on the HIFI instrument and its data reduction.

1.3.2 Heterodyne Instrument for the Far-Infrared (HIFI)

The Heterodyne Instrument for the Far-Infrared (HIFI[2]) is an ultra high spectral resolution heterodyne spectrometer with frequency ranges covering from 480–1250 GHz and 1400–1900 GHz (Fig. 1.8). Due to the high water content of the Earth's atmosphere, these wavelengths mostly cannot be observed with ground-based telescopes. HIFI's core scientific goals are to study the ISM in the Milky Way and other galaxies; stellar evolution, especially the formation and the late stages; and Solar System. Some of the key molecules that are targeted are H_2O, O_2, CO, OH, and HDO.

[2] Technical information about HIFI can be found in the "HIFI Observers Manual" and "HIFI Users Manual" from the ESA website.

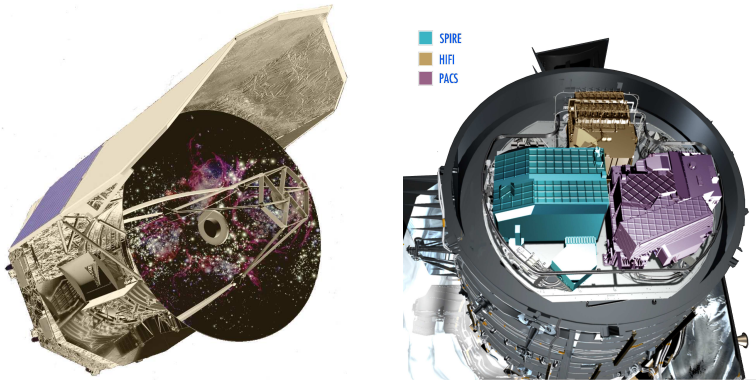

Figure 1.7 – *(Left:) Herschel* Space Observatory and *(right:)* its three on-board instruments, HIFI, PACS, and SPIRE (Image Credits: ESA).

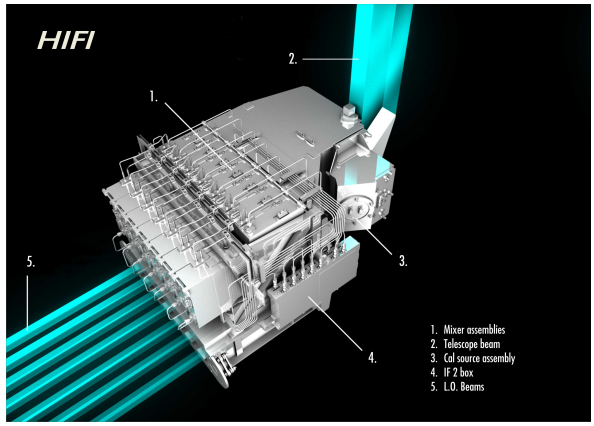

Figure 1.8 – Focal plane unit of the Heterodyne Instrument for the Far-Infrared (HIFI) instrument. Image Credit: ESA

HIFI has seven mixer bands (Bands 1–7) with horizontal (H) and vertical (V) polarizations. Bands 1 to 5 are using heterodyne SIS (Superconductor-Insulator-Superconductor) mixers to operate at 480–1250 GHz. Bands 6 and 7 use HEB (Hot Electron Bolometer) mixers for covering 1400–1900 GHz, which is better suited to detect radiation above 1000 GHz. In Table 1.1, the frequency ranges of the HIFI bands, the type of the mixers used, and the observed transitions that were used in this thesis are tabulated.

An instantaneous frequency coverage of 4 GHz is provided for Bands 1 to 5 and 2.4 GHz in Bands 6 and 7. The data are obtained as dual sideband data (DSB), which means that each channel of the spectrometers is sensitive to two frequencies (separated by 4.8 to 16 GHz) at the same time. This principle is explained in the next subsection. There are four spectrometers on board HIFI;

Table 1.1 – Overview of the HIFI bands

HIFI Band	Frequency (Min)[GHz]	Frequency (Max) [GHz]	Mixer	Observed Molecules[a]	HPBW (Min)["]
Band 1a	487.6	553.4	SIS	O_2, $C^{18}O$ 5–4	44
Band 1b	562.6	628.4	SIS	...	38
Band 2a	634.1	717.9	SIS	...	34
Band 2b	722.1	793.9	SIS	...	30
Band 3a	807.1	851.9	SIS, Diplexer	...	27
Band 3b	866.1	952.9	SIS, Diplexer	^{13}CO 8–7	25
Band 4a	957.2	1052.8	SIS, Diplexer	$C^{18}O$ 9–8	22
Band 4b	1054.7	1113.8	SIS, Diplexer	^{13}CO, $C^{18}O$ 10–9	20
Band 5a	1116.2	1235.8	SIS	^{12}CO 10–9	19
Band 5b	1235.2	1271.8	SIS	...	17
Band 6a	1430.2	1557.8	HEB, Diplexer	...	15
Band 6b	1578.2	1697.8	HEB, Diplexer	...	13
Band 7a	1701.2	1793.8	HEB, Diplexer	...	13
Band 7b	1793.2	1901.8	HEB, Diplexer	...	12

Notes: [a] The molecules that are observed and analysed in this thesis.

two Wide-Band Acousto-Optical Spectrometers (WBS) and two High Resolution Autocorrelation Spectrometers (HRS) each with H- and V polarizations. The observations are conducted for each of the spectrometers simultaneously. The WBS covers the full intermediate frequency bandwidth of 2.4 GHz in the highest frequency bands (Bands 6 and 7) and 4 GHz in all other bands at a single resolution (1.1 MHz ~0.2–0.7 km s^{-1}). The HRS have variable resolution from 0.125 to 1.00 MHz with subbands sampling up to half the 4 GHz intermediate frequency range. Subbands have the flexibility of being placed anywhere within the 4 GHz range. The HRS can be split up to allow the sampling of more than one part of the available range (for detailed information, see "*HIFI Users Manual*[3]" and "*HIFI Observers Manual*[4]"). The beam size (HPBW) of HIFI ranges from 42″ at 480 GHz to 12″ at 1900 GHz (Table 1.1). The in-flight performance and the calibration of HIFI are described in Roelfsema et al. (2012).

Heterodyne principle

Submillimeter wavelengths lie in between IR and radio wavelengths. The optical technology is very good in the near-IR side of the spectrum and on the other hand, electronics are quite advanced on the radio side of the spectrum. However, there is no direct method to amplify weak signals at submillimeter wavelengths. The solution to this problem is accomplished with the *heterodyne technique*, by bringing the signal down in frequency to radio wavelengths without losing its information from the original sky signal.

HIFI uses heterodyne technology in order to observe at far-infrared and submillimeter wavelengths at very high spectral resolution (resolving power of $\lambda/\Delta\lambda \sim 10^6$). In Fig. 1.9, a basic diagram of a submillimeter telescope is shown. In principle, the signal from an astronomical source at a frequency ν_{sky} (e.g., 812 GHz) is caught by the highly accurate mirror (dish), and it is mixed with

[3] `http://www.sron.rug.nl/hifi_icc/hifi-um/hifi-um.html`
[4] `http://herschel.esac.esa.int/Docs/HIFI/html/hifi_om.html`

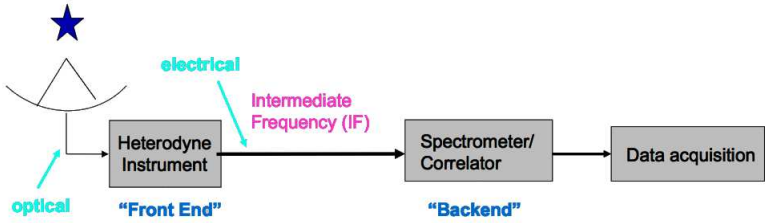

Figure 1.9 – Representative basic diagram of a submillimeter telescope.

a constant signal that is artificially generated by the local oscillator (LO) $\nu_{\rm LO}$ (e.g., 807 GHz). The mixing is done in the heterodyne receiver via high technology mixers at superconducting temperatures. The output electrical signals contain the sum and the difference frequencies at $\nu_{\rm LO}+\nu_{\rm sky}$ and $\nu_{\rm LO}$-$\nu_{\rm sky}$. Although the sum frequency component is filtered away, however, the difference frequency component produces the intermediate frequency $\nu_{\rm IF}$ (e.g., 5 GHz), which is then sent to HIFI's WBS and HRS spectrometers for the spectral analysis (de Graauw et al. 2010, Roelfsema et al. 2012).

Observing modes

In HIFI, three *Astronomical Observing Templates* (AOTs) are available in order to perform observations: *Single Pointing:* (AOT I) for observing astronomical sources at one position on the sky; *Mapping:* (AOT II) for observing extended regions; and *Spectral Scanning:* (AOT III) for surveying a single position on the sky over a continuous range of frequencies selected within the same LO band. Each of these AOT's can be used in a variety of different observing modes to provide the best quality data. The HIFI observing modes are:

Dual Beam Switch (DBS): Internal chopper mirror within HIFI is used to move the beam to a reference position up to 3 arcmin away from the target position. It is best used for non-crowded regions.

Position Switch (PSw): The HIFI beam is pointed to clean reference position, which is selected in a nearby region to the target.

Frequency Switch (FSw): The LO frequency is shifted by a small amount (a few tens of MHz), and the lines of interest still remain observable at two LO frequencies.

Load Chop: An internal cold source is used as a reference and the chopping mirror alternately looks at the target on the sky and an internal source of radiation.

In this thesis, we only used data of single pointing observations conducted primarily with "Dual Beam Switch (DBS)" or "Position Switch" observing modes.

HIFI noise characteristics

In this subsection, some tests of the data quality are presented. The aim was to quantify the behavior of the noise with increasing integration time in HIFI via analysing deep single pointing observations of different bands. In particular, the *rms* is expected to decrease with increasing integration time as $\sqrt{1/t}$ so several samples of long integration observations were used to test this. The observations are re-pipelined to Level 2 stage by removing the `doAvg` step in Level 1 tasks,

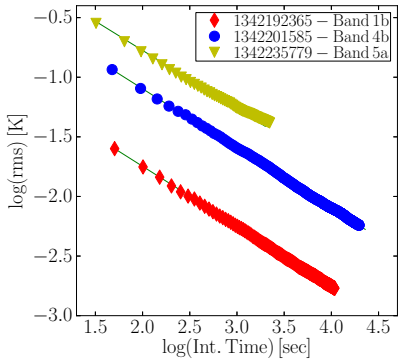

Figure 1.10 – Slopes show the decreasing *rms* with increasing integration time. The green lines behind the observed points show the expected *rms* evolution following $\sqrt{1/t}$ to indicate the expected behavior.

which then process all individual on-target data into Level 2 spectra with proper frequency scale and calibration. Since all individual on-target spectra are consecutive in time, the applied method is as follows: the first observed spectrum is taken and the *rms* is calculated, then the next spectrum is averaged with the first two (1^{st}+2^{nd}) and the *rms* is calculated again. Then the third spectrum is averaged with the previously averaged spectra (1^{st}+2^{nd}) and the *rms* is calculated, and so on. This process is continued by adding the next spectrum to the previously averaged spectra until the final spectrum. Figure 1.10 shows examples of *rms* versus integration time on three observations; e.g, obsid-1342192365 is a Band 1b observation, obsid-1342201585 is a Band 4b observation, and obsid-1342235779 is a Band 5a observation. All these observations are conducted in DBS FastChop mode. The green line shows the expected *rms* evolution following $\sqrt{1/t}$ for easy comparison. The slopes clearly show that the noise goes down with the increasing integration time, even long integrations of several hours. This is important to reach many of the HIFI science goals, including the search for O_2.

1.3.3 Ground-based telescopes

Atacama Pathfinder EXperiment

The Atacama Pathfinder EXperiment (APEX[5]) is a 12-meter submillimeter telescope at an altitude of 5100 meters at Llano de Chajnantor in Chile (Fig 1.11 *left*). It has various instruments operating from ~200 GHz up to THz frequencies. In this thesis, we primarily used the CHAMP$^+$ instrument (Kasemann et al. 2006, Güsten et al. 2008) in order to observe high-J CO lines (J_{up}= 6 up to 8). It is a PI instrument built by Max Planck Institute for Radioastronomy, Germany (PI: R. Güsten) with contribution from SRON-Groningen, the Netherlands. The instrument consists of two heterodyne receiver arrays, each with seven pixel detector elements for simultaneous operations in the 620–720 GHz and 780–950 GHz frequency ranges. The APEX beam sizes correspond to 8″ at 809 GHz and 9″ at 691 GHz. Its state-of-the-art technology combined with excellent atmospheric conditions at the site makes the instrument ideal to observe high-frequency molecular transitions.

[5] This thesis is based on data acquired with the Atacama Pathfinder Experiment (APEX). APEX is a collaboration between the Max-Planck-Institut für Radioastronomie, the European Southern Observatory, and the Onsala Space Observatory.

Figure 1.11 – *Left:* 12-m APEX telescope located at the Cerro Chajnantor plateu at 5100-m altitude. *Right:* 15-m JCMT located at Mauna Kea, Hawaii. Photo Credits: Umut Yıldız.

A detailed description of the instrument and observations of several sources in the current sample have been presented in van Kempen et al. (2009a,b,c), Yıldız et al. (2012, in prep (Chapter 4)). Maps of the ^{12}CO 6–5, 7–6 and ^{13}CO 6–5 lines over a few arcmin region were observed for all *Herschel* sources visible from Chajnantor, whereas ^{13}CO 8–7 and C^{18}O 6–5 lines were obtained for selected objects in staring mode. In addition, lower-J transitions were observed for southern sources using various receivers at APEX (van Kempen et al. 2006, 2009a,b,c). These new high-J CO observations along with molecular line surveys probe the velocity structure, physical conditions, and molecular abundances of dense gas around the protostars.

James Clerk Maxwell Telescope

The James Clerk Maxwell Telescope (JCMT[6]) is a 15-meter submillimeter telescope at an altitude of 4092 meters on Mauna Kea, Hawaii (Fig 1.11 *right*). Two instruments, HARP-B and RxA, are primarily used in order to observe low-J CO lines (e.g., 3–2 and 2–1) in this thesis. The HARP-B instrument (Dent et al. 2000, Smith et al. 2008, Buckle et al. 2009) is used to observe the 3–2 lines, which allows heterodyne spectroscopy with instantaneous mapping capability. The instrument consists of 16 SIS detectors with 4×4 pixel elements of 15″ each at 30″ separation. The tuning range is 325–375 GHz and it covers an area of 2′×2′ region in the sky. The beam size of each receptor is approximately 14″. RxA is a single-pixel double side band (DSB) receiver, operating between 211 and 276 GHz range. Our CO 2–1 lines were observed with RxA receiver with a beam size of ~23″. A fraction of the observations were obtained from the JCMT public archive[7] whereas the rest were obtained in dedicated campaigns.

1.4 WISH

[6] The JCMT is operated by The Joint Astronomy Centre on behalf of the Science and Technology Facilities Council of the United Kingdom, the Netherlands Organisation for Scientific Research, and the National Research Council of Canada.

[7] This research used the facilities of the Canadian Astronomy Data Centre operated by the National Research Council of Canada with the support of the Canadian Space Agency.

The "Water In Star-forming regions with *Herschel* (WISH[8])" is a 425 hours guaranteed time key-program on *Herschel* Space Observatory in order to study the physical and chemical structure of star-forming regions by focussing on H_2O and other related species (van Dishoeck et al. 2011). The project involves more than 80 international scientists in 35 institutes from 10 countries. The program covers ~80 sources in seven sub-programs with different luminosities ranging from low- (0.8 $L_\odot$) to high-mass protostars (10^5 $L_\odot$); and in different evolutionary stages from pre-stellar cores to protoplanetary disks. In the WISH project, high spectral and spatial resolution spectroscopy is obtained by using both HIFI and PACS instruments.

Water is the primary target in the project, because it is one of the most abundant key molecules in star-forming regions so its formation in different environments needs to be understood. It is a cornerstone in the oxygen chemistry network, which is the basis for many other chemical reactions. Conversely, water is an excellent tracer for probing different physical conditions since its abundance variations are very large: in cold regions the water abundance is very low, only 10^{-9}–10^{-8} with respect to H_2, whereas in hot regions, most of the gas-phase oxygen is locked in water with an abundance of ~10^{-4}. Water is also found to be an excellent tracer of the dynamical processes in outflows, which contain large amounts of water (Kristensen et al. 2011, Vasta et al. 2012, Santangelo et al. 2012). More information about the project can be found in the review articles of van Dishoeck et al. (2011) and Kristensen & van Dishoeck (2011), and the results of the individual subprograms can be found in the dedicated website[8].

When quoting envelope or outflow abundances, it is of course important to compare this abundance with respect to something. At outflow positions far from the central source, *Spitzer* Space Telescope data provide direct constraints on the H_2 column density from observations of low-J rotational lines in the mid-infrared. Towards the central source position, H_2 is not detected because the extinction is too high even at MIR wavelengths (Maret et al. 2009). CO is a chemically stable molecule with many transitions at sub-mm and mm wavelengths. Therefore, observations of CO in many rotational transitions can provide the reference frame for the column densities of cold, warm, and hot gas, and thereby a reference frame against which to measure the H_2O abundance as well as that of other species, e.g., O_2.

This thesis is based on the data observed with HIFI in the low-mass subprogram. In total, the sample contains 29 low-mass Class 0 and Class I sources. The sample selection criteria with the coordinates and other basic information of the source list are presented in van Dishoeck et al. (2011) with updates in Kristensen et al. (2012). The low-mass sources are located in various nearby molecular clouds, e.g., the Perseus, Ophiuchus, Taurus, and Serpens molecular clouds. Fortunately, as it turns out, several CO and isotopolog transitions fall close to H_2O transitions making it possible to observe them in one setting and thereby maximizing telescope efficiency. These include: ^{13}CO 10–9 with H_2O 1_{11}–0_{00} (40 min); $C^{18}O$ 5–4 with $H_2^{18}O$ 1_{10}–1_{01} (60 min); $C^{18}O$ 9–8 with H_2O 2_{02}–1_{11} (20 min); and $C^{18}O$ 10–9 with H_2O 3_{12}–3_{03} (30 min or 5 hours). An example setup is shown in Fig. 1.12, $C^{18}O$ 9–8 (987.56 GHz) with H_2O 2_{02}–1_{11} (987.92 GHz). Two CO surveys are presented in this thesis (Chapters 3 and 5)

1.5 WISH live data show

WISH HIFI data consist of either "Single Pointing" (DBS, PSw, FSw, LoadChop) or "Mapping" (OTF PSw, FSw) observations. The WISH observations were conducted between February 3, 2010 until February 25, 2012 by executing 821 AORs (Astronomical Observing Re-

[8] `http://www.strw.leidenuniv.nl/WISH/`

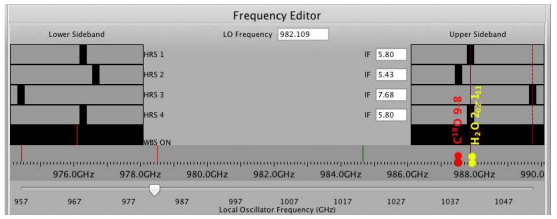

Figure 1.12 – WISH observations aim to cover as many lines as possible in one observing setup. The above example shows the setup for $C^{18}O$ 9–8 (987.56 GHz) with H_2O 2_{02}–1_{11} (987.92 GHz).

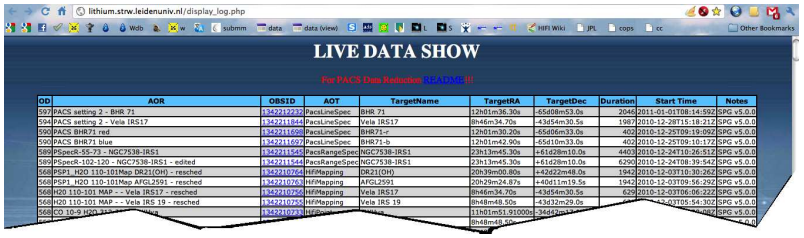

Figure 1.13 – A glimpse of "WISH Live Data Show" database that is available to the WISH team members.

quest). All the WISH proprietary data are collected in one computer at the Leiden Observatory. In order to provide easy and constant access to all WISH data by the team worldwide, a MySQL and Python powered database and HIFI data reduction pipeline has been constructed. This password protected database is called the "*WISH Live Data Show (LDS)*" (Fig. 1.13). Although the WISH project also contains PACS observations, PACS data are reduced by other team members and only collected in the LDS. The LDS data reduction pipeline primarily works for HIFI data, which interacts with the *Herschel* Science Archive (HSA), *Herschel* Interactive Processing Environment (HIPE), and GILDAS-CLASS softwares.

The database syncs with HSA for new observations every day. Then the pipeline downloads and reduces new HIFI data using the latest officially released HIFI pipeline, which therefore provides almost publication quality data 24 hours after the *Herschel* observations. The data are available in different formats, e.g., HIPE imported, CLASS, fits, and also quick image previews in png and eps format. We regularly check if HSA provides the data by using new pipelines, in that case all the observations are re-downloaded and re-reduced. In order to compare with old data reductions, nothing is deleted from the database, even data reduced with HIPE v.1.0 up to the latest version HIPE v.10.0 are available. Re-pipelining was done for all observations with the new calibration before publishing the HIFI first results papers in 2010 (HIPE v.1.x, v.2.x to HIPE v.3.0.1).

The steps in the pipeline are fully automatic, these include:

- Connecting to HSA *Observation Log* at 00:00 hrs
- Checking the new observations, if so, adding them to pipeline queue
- Connecting to HSA and importing data to HIPE
- Saving imported observation to disk
- Separating subbands of Level 2 data set

- Stitching the subbands
- Saving the stitched spectra as png and eps files
- Creating fits files for stitched and non-stitched spectra
- Converting fits files to GILDAS-CLASS format
- Creating webpages to display the output
- Updating the database if the pipeline is successful
- Saving all the output by adding the current date to filename in the "Log" folder

If re-pipelining, removing standing waves, or any other additional data manipulation is necessary, these steps are included after importing the data to HIPE. Re-pipelining starts from Level 0.5 data, which is mostly raw data but the data are processed such that backend (spectrometer) effects are removed and frequency calibrated. This database will become public after the WISH key program is finalized and it will be transferred to our legacy database `LOMASS`[9] (Leiden Observatory Single-dish Submm Spectral Database of Low-mass YSOs), which will archive thousands of spectra observed with many telescopes for many low-mass protostars.

1.6 This thesis

The primary focus of this thesis is the *formation of low-mass protostars*, specifically the earliest deeply embedded phase, when material from the collapsing envelope is still accreted onto the growing young star. A variety of state-of-the-art sub-/mm instruments are used for the observations in order to understand the physical and chemical nature of this phase, centered around the *Herschel* Space Observatory. Rotational transitions of molecules, specifically, low- and high-lying lines of CO and its isotopologs have been used to characterize the YSO structure and kinematics. The high frequency observations with *Herschel* allow much warmer gas to be probed than was possible previously. The following questions are addressed:

- How is CO excited in the different parts of the YSOs, and what are the locations and relative importance of shocks and UV heating? Can we quantify this '*feedback*' on the surroundings? How does this relate to what is seen in H_2O?
- Does the CO excitation and do the line characteristics change with evolution from the deeply embedded Class 0 YSOs to less deeply embedded Class I YSOs?
- What is the CO abundance structure throughout the envelope: where is CO frozen out and where does it evaporate? Is it processed to other molecules on the grains?
- What is the abundance of O_2 in protostellar environments? Why is it so anomalously low compared with CO?

These questions are addressed in the following chapters.

Chapter 2 — *Herschel*-HIFI observations of high-J lines (up to J_u=10) of ^{12}CO, ^{13}CO, and C^{18}O are presented toward three deeply embedded low-mass protostars in the NGC 1333 star-forming region. The observations show several energetic components including shocked and quiescent gas. The results are: (***i***) ^{12}CO line widths increase from lower-J toward higher-J transitions. (***ii***) CO and its isotopologues trace different material. The ^{12}CO 10–9 lines are dominated by broad ($FWHM$ 25–30 km s^{-1}) emission indicating a large-scale shock process (>1000 AU). Several CO and ^{13}CO line profiles reveal a medium-broad component (5–10 km s^{-1}), seen prominently in H_2O lines, indicative of small-scale shocks (<1000 AU). Narrow C^{18}O lines (2–3 km s^{-1}) trace the quiescent envelope material. (***iii***) Higher-J isotopologue lines (e.g., C^{18}O 9–8 and 10–9; E_{up}=237 and

[9] http://lomass.strw.leidenuniv.nl

289 K) probe high temperatures. However, analysis shows that for a power-law envelope at least 50% of the observed emission still comes from the colder <40 K parts of the envelope. Three different models using the RATRAN radiative transfer code are applied to the optically thin $C^{18}O$ lines to quantify the CO abundance. For the "*constant*" profile, the observed line intensities cannot all be reproduced simultaneously. For the "*anti-jump*" model, the outer abundance, X_0, was kept high for densities lower than the desorption density, n_{de}. It fits well the lower-J lines, but the higher-J lines are underproduced. In the "*drop*" model, the inner abundance, X_{in}, increases above T_{ev}. This model fits well all lines, however X_{in} is a factor of ~3-5 below X_0 for the best fit to the IRAS 2A data. This suggests that a significant fraction of the CO ice is transformed to other species on the grains.

Chapter 3 — This chapter builds on the results of Chapter 2 by presenting *Herschel*-HIFI observations of the same CO lines for a much larger sample of 26 deeply embedded low-mass Class 0 and Class I young stellar objects. This is the first large-scale spectrally resolved high-J CO survey ever conducted for these types of sources. Complementary lower-J CO maps were also observed using ground-based JCMT and APEX telescopes and convolved to matching beam sizes. The ^{12}CO 10–9 line is detected for all objects and can generally be decomposed into a narrow and broad component due to the quiescent envelope and entrained outflow material, respectively. The median excitation temperatures for ^{12}CO, ^{13}CO, and $C^{18}O$ derived from single-temperature fits to the J_{up}=2–10 integrated intensities are ~70 K, 48 K and 37 K, respectively, with no significant difference between Class 0 and Class I sources and no trend with M_{env} or L_{bol}. Thus, in contrast with the continuum SEDs, the spectral line energy distributions (SLEDs) do not show an evolution during the embedded stage. In contrast, the integrated line intensities of all CO isotopologs show a clear decrease with evolutionary stage as the envelope is dispersed.

Chapter 4 — Two well-known Class 0 low-mass protostars NGC 1333 IRAS 4A and IRAS 4B are mapped in the ^{12}CO 6–5 transition in order to characterize the warmer parts of the protostellar envelope using the new generation APEX-CHAMP$^+$ array receiver. This study allowed us to quantify the feedback of the protostars on their surroundings in terms of shocks, ultraviolet (UV) heating, photodissociation, and outflow dispersal. The map shows that the broad CO emission-line profiles trace entrained shocked gas along the outflow walls, which have an average temperature of ~100 K. At other positions surrounding the outflow and the protostar, the 6–5 line profiles are narrow indicating UV heating. The narrow ^{13}CO 6–5 data directly reveal this UV heated gas distribution for the first time. The amount of UV-photon-heated gas and outflowing gas are quantified from the combined ^{12}CO and ^{13}CO 6–5 maps and found to be comparable within a 20″ radius around IRAS 4A, which implies that UV photons can affect the gas as much as the outflows. Weak [C I] emission throughout the region indicates that there is a lack of CO dissociating photons. As for IRAS2A studied in Chapter 2, modeling of the $C^{18}O$ lines demonstrates the necessity of a "drop" abundance profile throughout the envelopes where the CO freezes out and is reloaded back into the gas phase through grain heating, thus providing quantitative evidence of the CO ice evaporation zone around the protostars. The inner abundances are less than the canonical value of $CO/H_2=2.7\times10^{-4}$, however, strengthening the conclusion that there is some processing of CO into other species on the grains.

Chapter 5 — Large-scale CO maps of 26 low-mass young stellar objects are obtained using APEX-CHAMP$^+$ (^{12}CO and ^{13}CO 6–5), together with JCMT-HARP-B (^{12}CO and ^{13}CO 3–2). The maps are high spatial and spectral resolution, particularly CO 6–5 maps have 9″ pixels thus resolving the morphology of the outflows. In this chapter, these maps are analyzed using the same

methods to determine the outflow parameters and the results are compared with higher-J CO lines obtained with *Herschel*. All sources in our sample show outflow activity via CO line wings. One of the key parameters, the outflow force, F_{CO}, is measured and correlations with other physical parameters are sought. F_{CO} versus L_{bol} plots show that Class 0 sources have more powerful outflows than the Class I sources, even if their luminosities are comparable. Overall, the various outflow parameters indicate reduced outflow activity with evolutionary stage, consistent with previous studies. F_{CO} is directly proportional with M_{env} and M_{CO}, indicating that higher outflow forces require higher envelope masses and involve higher outflow masses. Comparison with high-J CO lines probed by PACS, which trace currently shocked gas, shows that although the 6–5 and PACS transitions do not probe the same gas component, the two components are still linked. However, the link does not extend down to CO 3–2. The conclusion is that CO 6–5 depends on the shock characteristics (pre-shock density and velocity), whereas CO 3–2 is more sensitive to conditions in the surrounding environment (density).

Chapter 6 — *Herschel*-HIFI observations of molecular oxygen, O_2, at 487 GHz toward the deeply embedded low-mass Class 0 protostar, NGC 1333-IRAS 4A, are presented. The deep HIFI spectrum fails to detect O_2 at the velocity of the dense protostellar envelope, implying one of the deepest upper limits of O_2/H_2 at $\leq 6\times10^{-9}$ (3σ). However, a tentative (4.5σ) detection of O_2 is seen at the velocity of the surrounding NGC 1333 molecular cloud, shifted by 1 km s^{-1} relative to the protostar. Pure gas-phase models and gas-grain chemical models overproduce O_2 in the dense envelope, unless a long pre-collapse stage ($\sim10^6$ years) is included, during which atomic and molecular oxygen are frozen-out onto the dust grains and fully converted into H_2O. These results imply that the gas and ice that enter protoplanetary disks are poor in O_2.

1.7 Future outlook

Further advances in our understanding of star formation will come from new technologies for high-frequency or highly efficient observations. Single dish millimeter telescopes will include instruments with many pixel detectors (e.g., 64-pixel heterodyne SuperCam at 345 GHz on the Sub-Millimeter Telescope). These array receivers will make it possible to produce large scale velocity maps of star-forming clouds that complement the big *Herschel* continuum surveys. This will aid in deciphering how dense cores form out of the larger filamentary structures seen in the Herschel images and how they eventually lead to the formation of individual stars or groups of stars.

On the other hand, the newly inaugurated Atacama Large Millimeter/ submillimeter Array (ALMA), the revolutionary interferometric observatory at an altitute of 5100 meters, opens up an entirely new era in the study of protostars, from low to high mass. Its 66 antennas with baselines ranging up to 16 km provide unprecedented sensitivity and angular resolution, down to 1 AU in the nearest star-forming regions. When working at full capacity, it will be well suited to unravel the physical mechanisms behind the formation of protostellar jets and outflows. Also, knowledge of binary star formation in the earliest deeply embedded phase is still lacking and the interactions of the outflows of binaries can only be disantangled with these high precision instruments. Thus, star formation research poses many interesting questions that can be answered in the coming years, highlighting its bright and exciting future.

Acknowledgements

I would like to thank to Carolyn McCoey, Ian (Max) Avruch, Per Bjerkeli and Robin Lombaert for their help on the HIFI noise report, and Erik Deul for setting up the MySQL system for our WISH database.

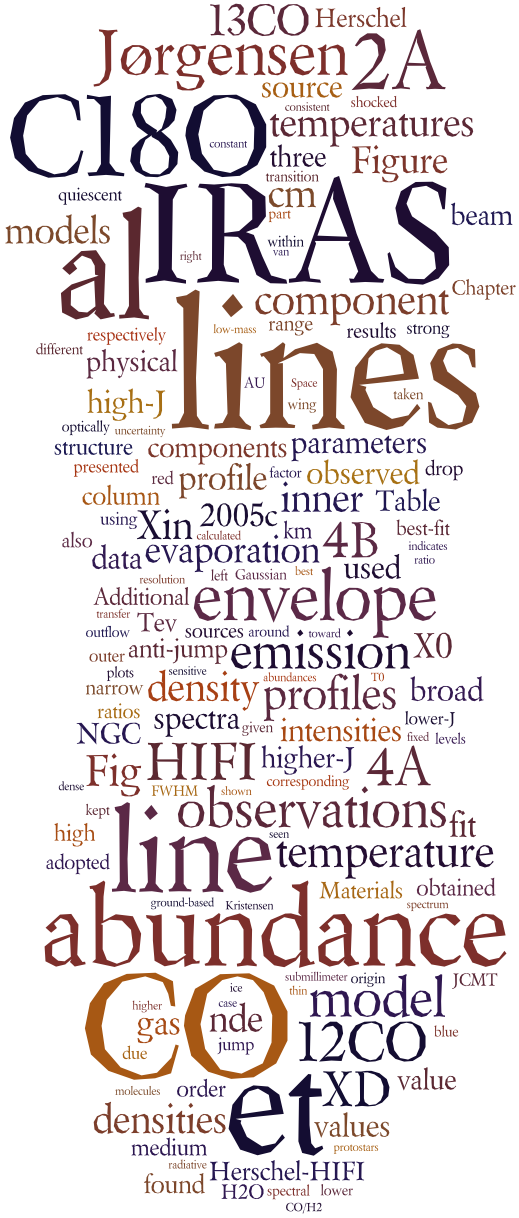
13CO
Herschel
Jørgensen
2A
source
shocked
consistent
C18O
temperatures
constant
three
Figure
transition
quiescent
cm
IRAS
beam
models
part
within
van
right
all
component
Chapter
low-mass
range
results
strong
respectively
different
physical
lines
AU
Space
wing
taken
high-J
optically
uncertainty
structure
components
parameters
presented
red
profile
factor
observed
drop
column
inner
Table
using
Xin
2005c
calculated
km
best-fit
indicates
ratio
also
data
evaporation
4B
used
left
Gaussian
best
resolution
Additional
envelope
transfer
Tev
sources
around
toward
outflow
outer
anti-jump
emission
X0
plots
sensitive
abundances
T0
narrow
density
profiles
broad
ratios
spectra
given
intensities
lower-J
fixed
levels
NGC
Fig
HIFI
higher-J
4A
dense
FWHM
shown
corresponding
kept
observations
fit
high
seen
line
temperature
adopted
Materials
obtained
ground-based
Kristensen
spectrum
abundance
submillimeter
origin
JCMT
thin
ice
CO
model
higher
case
gas
nde
12CO
blue
jump
due
molecules
order
et
XD
value
densities
values
medium
protostars
radiative
Herschel-HIFI
found
H2O
spectral
lower
CO/H2